Journal of Cleaner Production 356 (2022) 131854

Contents lists available at ScienceDirect

Journal of Cleaner Production

journal homepage: www.elsevier.com/locate/jclepro

One-step synthesis of nanoscale zero-valent iron modified hydrophobic mesoporous activated carbon for efficient removal of bulky organic pollutants

Qingxin Xu [a,b], Xuejiao Liu [a,**], Dengguo Lai [a], Zhenjiao Xing [a], Pamphile Ndagijimana [a], Zhiwei Li [a], Yin Wang [a,c,*]

[a] CAS Key Laboratory of Urban Pollutant Conversion, Institute of Urban Environment, Chinese Academy of Sciences, Xiamen, 361021, China
[b] University of Chinese Academy of Sciences, Beijing, 100049, China
[c] Ningbo (Beilun) Zhongke Haixi Industrial Technology Innovation Center, Ningbo, 315000, China

ARTICLE INFO

Handling Editor: Panos Seferlis

Keywords:
Hydrophobicity
Mesoporous activated carbon
Nanoscale zero-valent iron
One-step synthesis
Bisphenol A
Adsorption mechanism

ABSTRACT

It is of vital importance for industrial applications by developing simple, robust, economic, eco-friendly and easy scale-up methods for fabricating hydrophobic mesoporous activated carbon (MAC) from sustainable raw materials with high adsorption performance for bulky organic pollutants removal. Herein, a novel one-step facile approach coupling carbothermal reduction with catalytic activation was firstly established for preparing the coconut shell-based hydrophobic MAC modified with nanoscale zero-valent iron (NZVI@MAC). The in-situ synthesized NZVI (merely 0.33 wt%) by carbothermal reduction could not only catalyze the gasification reaction between carbon and CO_2 to fabricate MAC (d_{BET} = 5.17 nm, S_{BET} = 933.12 $m^2\ g^{-1}$), but also catalyze the amorphous carbon to form hydrophobic graphitic layers covering its surface. In striking contrast to the unmodified activated carbon, the NZVI@MAC surprisingly exhibited a remarkably 8.62-fold higher initial adsorption rate and a slightly increased adsorption capacity of 327.60 mg g^{-1} for bisphenol A (BPA). Intriguingly, the high mesoporous proportion (70–90%) of NZVI@MAC with the average pore size of 4.1–5.2 nm was effective in reducing the diffusion resistance for BPA. Such high adsorption performance under neutral conditions was primarily attributed to the strong hydrophobic interaction, π-π interaction and the weak hydrogen bonding. Moreover, the NZVI@MAC showed robust anti-interference properties in actual environmental conditions containing various inorganic ions and in a wide pH range (3–10). Therefore, the cost-effective, eco-friendly, sustainable and recyclable hydrophobic NZVI@MAC with stable structure and excellent performance for bulky organic adsorption is a promising material for practical applications, especially in drinking water purification.

1. Introduction

Nowadays, the increasing number of emerging pollutants have been frequently detected in groundwater, surface water, and even household drinking water (Careghini et al., 2015; Jeirani et al., 2017; Kang et al., 2006; Padhye et al., 2014). Bisphenol A (BPA, 0.43 × 0.53 × 0.70 nm^3) is an endocrine disruptor and one of the most produced and consumed chemicals around the world, which negatively affects the health and reproduction system of organisms at a low concentration of less than 1 μg m^{-3} (Flint et al., 2012). Adsorption technology, such as using activated carbon (AC) as adsorbent, is a promising technology to remove such pollutants in water at a ppm or even ppb level concentration (Jeirani et al., 2017; Ji et al., 2010). Since the adsorption performance of an adsorbent is tightly related to the physical structures (*e.g.*, total surface area, match between pore size of adsorbent and structure of adsorbate) and surface chemical properties (*e.g.*, functional groups, heteroatoms and compounds), a hydrophobic adsorbent with high mesoporous proportion is able to efficiently remove bulky organic pollutants because most of them are hydrophobic.

As a new generation of carbonaceous adsorbents, ordered mesoporous carbon (OMC) replicated by a hard-/soft-templating way has been developed with a uniform and tunable mesoporous structure (2–50

* Corresponding author. Institute of Urban Environment, Chinese Academy of Sciences, 1799 Jimei Road, Xiamen, 361021, China.
** Corresponding author. Institute of Urban Environment, Chinese Academy of Sciences, 1799 Jimei Road, Xiamen, 361021, China.
E-mail addresses: xjliu@iue.ac.cn (X. Liu), yinwang@iue.ac.cn (Y. Wang).

https://doi.org/10.1016/j.jclepro.2022.131854
Received 30 November 2021; Received in revised form 20 March 2022; Accepted 17 April 2022
Available online 19 April 2022

nm), a large surface area and a high pore volume. A magnetic OMC with a dual-size mesoporous structure (2.8–2.9 and 3.5–4.1 nm) and large specific surface areas (975–1321 $m^2\ g^{-1}$) showed an excellent adsorption capacity for bulky dyes, such as methylthionine chloride, methyl orange, rhodamine and Congo red (Dong et al., 2012). The adsorption amount was suggested to depend on the total surface area and the match of structure and size between adsorbent and adsorbate. The introduction of nitrogen-containing functional groups covering the surface of OMC could significantly increase its hydrophobicity, which significantly improved the removal efficiency of ciprofloxacin compared with OMC (Peng et al., 2015). Despite the OMC being regarded as an appropriate material for the adsorption of bulky adsorbates, its preparation requires to use a large number of chemical reagents, and its technology is relatively sophisticated at a high cost up to 339.50 $\$\ kg^{-1}$ (Lian et al., 2020). The practical application of hydrophobic mesoporous materials mainly depends on not only its high adsorption capacity and efficiency but also its simple, stable, cost-effective and green synthesis process.

Coconut shell is an ideal natural waste material for AC production due to its low ash content, high mechanical strength and special texture. It has been reported that chemical and catalytic activation can be used to prepare mesoporous AC (MAC) compared with physical activation. In the chemical activation method, chemical reagents, such as H_3PO_4 (Hadoun et al., 2013), H_2SO_4 (Rahman et al., 2019), $ZnCl_2$ (Hu and Srinivasan, 2001), NaOH and KOH (Liew et al., 2018), are commonly used to produce MAC. However, these reagents are highly corrosive to equipment and hazardous causing severe environmental pollution, and the hazardous chemical residues in the as-prepared materials are also difficult to be completely removed, which greatly limits the practical applications in environmental treatment. For the catalytic activation method, transition metals (*e.g.,* Fe, Co, Ni) (Hong et al., 2000) and alkaline/alkaline earth metals (*e.g.,* Li, Na, K, Ca, Sr, Ba) (Suzuki et al., 1994) are often selectively used to catalyze the gasification reaction of carbon with H_2O or CO_2. The catalytic process is under a relatively mild condition in comparison with the chemical activation, although some metal residues can be left in the MAC.

Among these metals, nanoscale zero-valent iron (NZVI) with high specific surface area, non-toxicity, and strong reducibility ($E_0 = -0.44$ V) is highly effective to remove and degrade a variety of environmental pollutants, such as organic compounds containing nitro or halogen functional groups (Oh et al., 2017), dyes (He et al., 2012), inorganic heavy metals (Dai et al., 2016) and phosphate (Zhou et al., 2014), nitrates (Wang et al., 2021). Liu et al. (1999) synthesized the pitch-based MAC using H_2O activation with the aid of ferrocene. Qiao et al. (2005) converted AC into MAC through CO_2 gasification by impregnating AC with iron nitrate. Subsequently, the obtained MAC could be modified with hydrophobic substances, such as docosahexaenoic acid (Kaur et al., 2019), docosahexaenoic acid (Lei et al., 2013), Polydimethylsiloxane (Li et al., 2020). However, these preparation approaches were normally complex and costly, and required high energy and time consumption due to the multiple steps.

Herein, for the first time, we proposed a novel one-step approach by coupling carbothermal reduction with catalytic activation to prepare the ultralow NZVI modified hydrophobic MAC (NZVI@MAC) using the renewable agricultural waste of coconut shell as raw materials. Importantly, the fabrication process was simple, robust, eco-friendly and low cost with low energy- and time-consumption, which was suitable for mass production. The in-situ synthesized NZVI was highly dispersed and embedded on the surface of MAC ($d_{BET} = 5.17$ nm, $S_{BET} = 933.12$ mg g^{-1}), resulting in a gradient pore structure with a strong hydrophobic property. Relative to the unmodified conventional AC, the NZVI@MAC exhibited a remarkable 8.62-fold increase in the initial adsorption rate with a slightly higher adsorption capacity of 327.60 mg g^{-1} for BPA. Furthermore, the synthesis condition of NZVI@MAC was optimized, and the underlying relationships and mechanisms behind the interaction of pore structure, chemical property of NZVI@MAC with adsorption performance were comprehensively investigated. Its anti-interference properties in actual environmental conditions containing various interfering ions and in a wide pH range was conducted. Finally, the reaction mechanism was investigated, and the safety and regenerability of NZVI@MAC were also assessed. This work was useful to design similar carbon materials for adsorption.

2. Materials and methods

2.1. Materials and reagents

The commercial carbonized coconut shell, purchased from Jiangsu Youhuada Environmental Protection Material Technology Co., LTD, was ground and sieved to collect the particles in the size of 40–60 meshes. The sample was dried after washing with deionized water. BPA (purity >99%) and triclosan (purity = 97%) were purchased from Aladdin (Shanghai, China), the other reagents were purchased from Sinopharm Chemical Reagent Co., LTD. The deionized water was used for all experiments.

2.2. Synthesis procedures

A certain amount of $Fe(NO_3)_3{\cdot}9H_2O$ based on Fe^{3+} to carbonized materials (0.1–1.0 wt%) was dissolved in the water/ethanol mixture (0.25–4: 1, v: v). Subsequently, 10 g of carbonized coconut shell was added to the ferric solution, followed by stirring for 24 h at 400 r min^{-1} before filtering and drying. Eventually, the Fe^{3+}-doped carbonized materials were transferred into a stainless-steel tube for activation by heating at 6 °C min^{-1} under N_2 atmosphere (0.4 L min^{-1}). Once the temperature was up to the setpoint (750–850 °C), the atmosphere was rapidly shifted from N_2 to CO_2 or H_2O maintained for a certain time (60–100 min). The activation device was cooled down to room temperature under the N_2 protection before collecting the synthesized NZVI@MAC. NZVI was synthesized by liquid phase reduction (Text S1).

2.3. Characterization

The iron phase and the crystalline structure of the samples were analyzed by X-ray diffraction (XRD, X'Pert Pro, Netherlands) with a Rigaku D/MAXYA diffractometer and Cu-Ka radiation. The thermal weight variation of the raw materials was estimated by thermal gravimetric analysis (TG/DTG, Netzsch TG 209 F3, Germany) from 40 to 900 °C under N_2 and CO_2 atmosphere at 10 °C min^{-1}. The morphology was examined by scanning electron microscopy (SEM, Hitachi S-4800, Japan) and transmission electron microscope (TEM, JEOL JEM2100, Japan). The elemental distribution was performed by an energy dispersive spectrometer (EDS) coupled in SEM. The pore structure was measured by the N_2 adsorption-desorption isotherm at 77K (TriStar II 3020 and AutoChem II 2920, USA), and calculated by Brunauer-Emmett-Teller (BET) and Barrett-Joyner-Halenda (BJH) methods. Raman spectra was collected by a Laser Raman spectrometer (Raman, LabRAM Aramis, France). The surface function groups were identified by the Fourier transform-infrared spectroscopy (FTIR, Nicolet iS10, USA). The point of zero charge was conducted by zeta potential analyzer (Zeta, Zeta PALS, UK), and the pretreatment method of sample was described in Text S2. The concentration of Fe was determined by Inductively Coupled Plasma Mass Spectrometry (ICP-MS, Agilent 7700).

2.4. Batch experiments

To acquire the adsorption capacity, the solution with higher BPA concentrations than that of actual tap water were used in this study. In a typical adsorption process, the adsorbent (0.2 g L^{-1}) and BPA (60 mg L^{-1}) were added into a 250-mL amber flask. The mixture was shaken at 298.15 K, 160 r min^{-1}. For the kinetics studies, the supernatant was withdrawn and filtered through a 0.22 μm PTFE membrane at a certain time interval. For the isotherm studies, the adsorbent (0.2 g L^{-1}) and

BPA (50–120 mg L^{-1}) were mixed at a controlled temperature between 298.15 and 318.15 K. The residual concentration of BPA was detected using a UV spectrophotometer (UV-1100, MAPADA, China) at 276 nm. All experiments were conducted in duplicate or triplicate. The information of all equations and models was detailed in Text S3.

2.5. Desorption and regeneration

To evaluate the regeneration performance of the saturated NZVI@MAC, BPA desorption was tested with the aqueous solution at different pH and the organic solvents. Generally, 20 mg of the saturated NZVI@MAC was soaked into 100 mL of elution solution and shaken for 24 h at 160 r min^{-1}. Next, the NZVI@MAC was filtered and washed by deionized water, then dried for the following adsorption-desorption cycles.

3. Results and discussion

3.1. Preparation of hydrophobic NZVI@MAC

Carbothermal reduction and catalytic activation as a novel one-step approach was established to fabricate the hydrophobic NZVI@MAC. The carbonized coconut shell was selected as the raw materials, which was difficult to interfere with the fabrication process because most of volatile substances in the coconut shell had already been removed during the initial carbonization process. Using the water/ethanol mixture as dispersant, the impregnated Fe^{3+} was uniformly loaded on the surface of carbonized materials. The in-situ synthesized NZVI by carbothermal reduction (Eqs. (1)–(3)) (Jiang et al., 2019; Shen, 2015) could catalyze the gasification reaction between CO_2 and carbon (Eq. (4)) to fabricate the MAC, and the amorphous carbon to form hydrophobic graphitic layer covering its surface. The one-step synthesized hydrophobic NZVI@MAC by a convenient, cost-effective, eco-friendly and easy scale-up procedure could significantly improve the adsorption capability for BPA, and easily be separated and reused.

$$Fe(NO_3)_3{\cdot}9H_2O \rightarrow 2Fe_2O_3 + 12NO_2\uparrow + 3O_2\uparrow + 9H_2O\uparrow \quad (1)$$

$$6Fe_2O_3 + C \rightarrow 4Fe_3O_4 + CO_2\uparrow \quad (2)$$

$$2Fe_3O_4 + C \rightarrow 6Fe^0 + CO_2\uparrow \quad (3)$$

$$CO_2 + C \xrightarrow{Fe^0} 2CO\uparrow \quad (4)$$

The details of the optimization process of the NZVI@MAC were systematically studied. XRD patterns in Fig. 1a illustrated that the formation of Fe^0 was achieved in the N_2 and CO_2 atmospheres. The diffraction peaks at 44.7° matched with the (110) facet of Fe^0 (JCPDS No. 06–0696). However, in the H_2O atmosphere, the peak at 35.5° was attributed to the (311) facet of Fe_3O_4 (JCPDS No. 19–0629). These phenomena indicated that the presence of CO_2 did not affect the formation of Fe^0.

The pore structure of the synthesized samples (Table 1) showed that both CO_2 and H_2O were effective activator in the preparation of plain microporous ACs (commercial AC as control). After Fe^{3+} impregnation,

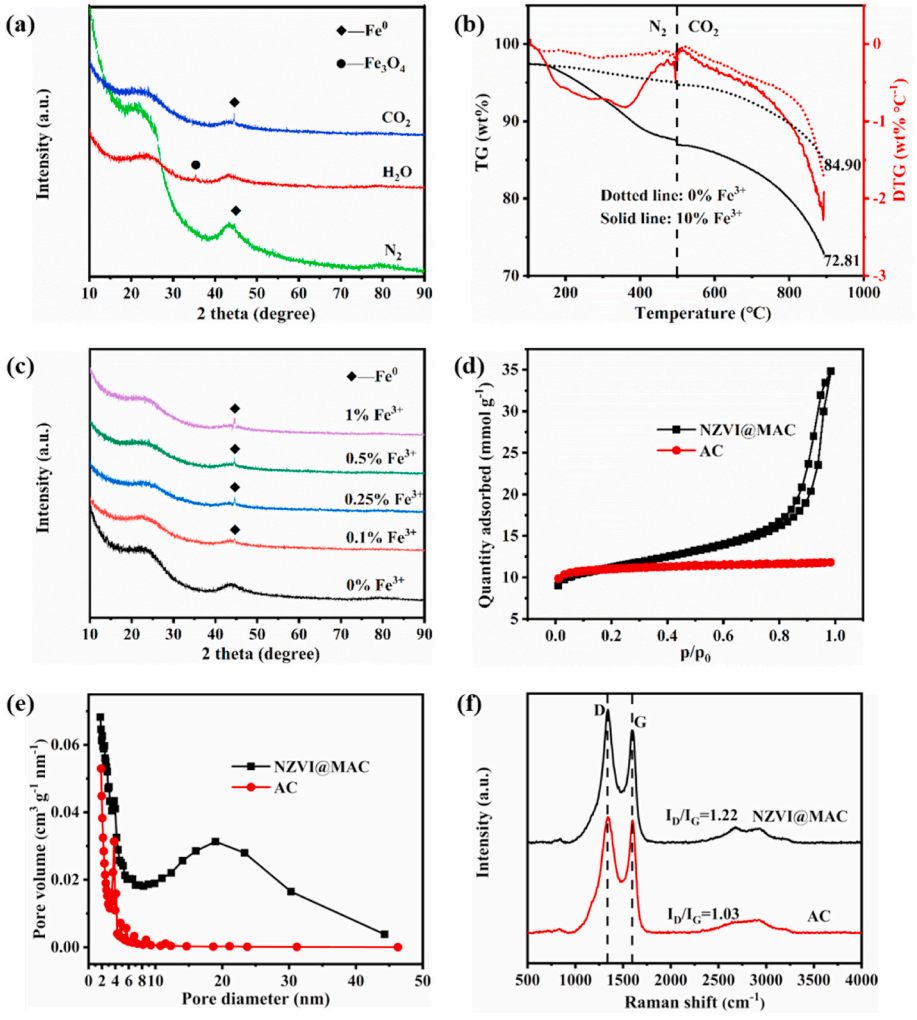

Fig. 1. Characterization of NZVI@MAC and reference AC. (a) XRD patterns of the adsorbents prepared in different atmospheres. (b) TG and DTG curves of the carbonized coconut shell impregnated with 0 and 10 wt% Fe^{3+} in the atmosphere changing from N_2 to CO_2 at 500 °C. (c) XRD patterns of the adsorbents prepared with different dosages of impregnated Fe^{3+} (wt%). (d) N_2 adsorption-desorption curves, (e) pore size distribution (a fake peak at 3–4 nm on AC) and (f) Raman spectra of NZVI@MAC and AC.

Table 1
The yield and pore structure characterization of the as-synthesized adsorbents.

Sample [a]	Yield (%)	S_{BET} (m^2 g^{-1})	V_{total} (cm^3 g^{-1})	S_{meso} (m^2 g^{-1})	V_{meso} (cm^3 g^{-1})	V_{meso}/V_{total} (%)	d_{BET} (nm)	d_{BJH} (nm)
Carbonized coconut shell	–	251.80	0.10	17.16	0.01	6.82	1.53	1.93
Commercial AC	–	964.49	0.41	147.89	0.06	15.33	1.70	2.50
AC-0-850-H_2O-80-0.3	43.27	1328.66	0.62	394.27	0.18	29.68	1.85	2.93
AC-0-850-CO_2-80-0.4	62.98	947.72	0.41	164.88	0.07	17.40	1.73	2.84
AC-0.5-850-N_2-80-0.4	85.41	94.24	0.06	55.41	0.03	58.80	2.34	2.59
AC-0.5-850-H_2O-80-0.3	39.94	1181.76	0.56	343.02	0.16	29.03	1.89	3.32
AC-0.5-850-CO_2-80-0.4	24.94	721.76	0.82	559.96	0.64	77.58	4.55	9.70

[a] AC-a-b-c-d-e represents AC synthesized with (a) the dosage of impregnated Fe^{3+}(wt%), (b) activation temperature (°C), (c) activator, (d) activation time (min), and (e) flow rate of activator (L min^{-1}).

the synthesis in the CO_2 atmosphere resulted in a significant increase in the average pore size from 1.73 to 4.55 nm with the mesoporous proportion increased from 17.40 to 77.58%. Meanwhile, the total pore volume was almost doubled to 0.82 cm^3 g^{-1}. This result revealed that CO_2 had a remarkable effect on the pore expansion in the presence of Fe^0. By comparison, the pore structure deteriorated in the N_2 atmosphere and the pore expansion almost could not be triggered in the H_2O atmosphere. These suggested that the Fe^0 played an important role in the pore expansion.

The thermogravimetric curves of the carbonized coconut shell impregnated with and without Fe^{3+} were shown in Fig. 1b. The weight loss of raw material was mainly related to the evaporation of water and the gradually escaped volatile (<500 °C). The accelerated thermal decomposition rate at high temperature (>700 °C) indicated the reaction rate between CO_2 with carbon increased. For the Fe^{3+} impregnated sample (10%), the main mass loss at 100–500 °C was attributed to the dehydrogenation of amorphous Fe species (*e.g.*, $Fe(OH)_3$ and FeO(OH)) to Fe_2O_3, and followed by the reduction to Fe_3O_4 (or less FeO) by reducing components (*e.g.*, amorphous carbon, H_2 and CO produced in the pyrolysis process) (Hoch et al., 2008; Jiang et al., 2019; Magalhães et al., 2009). Then the Fe^0 reduced at a higher temperature would catalyze the gasification reaction, resulting in a significant weight loss (>700 °C). Hence, the Fe^0 could lower the activation energy and shorten the gasification reaction time in the temperature range of 750–850 °C.

The synthesis conditions (dosages of impregnated Fe^{3+}, dispersants, activation temperatures, retention time, and flow rates of CO_2) of the NZVI@MACs were further optimized. XRD showed that Fe^0 synthesized in this study was dominant in Fe species, and its intensity increased gradually with the dosage of impregnated Fe^{3+} (Fig. 1c). The signals of Fe^0 could be detected except for 750 °C (Fig. S1a), which may be related to the higher yield of as-synthesized material (the concentration of Fe^0 was below the detection limit) because the intensified signal of Fe^0 could be discovered when the temperature was up to 600 °C (Jiang et al., 2019). The porosities (micro- and meso-porous) of the samples could be well tuned shown in Table S1. Given the production cost, the optimal synthesis condition including 0.25 wt% of impregnated Fe^{3+} with 4: 1 of V_{H2O}: $V_{ethanol}$ as dispersant. The reaction was activated at 850 °C for 80 min under the CO_2 atmosphere (0.4 L min^{-1}). The obtained sample, named as NZVI@MAC, offered 82.41% mesoporous (D_{BET} = 5.17 nm) with a high specific surface area of 933.12 m^2 g^{-1} and total pore volume

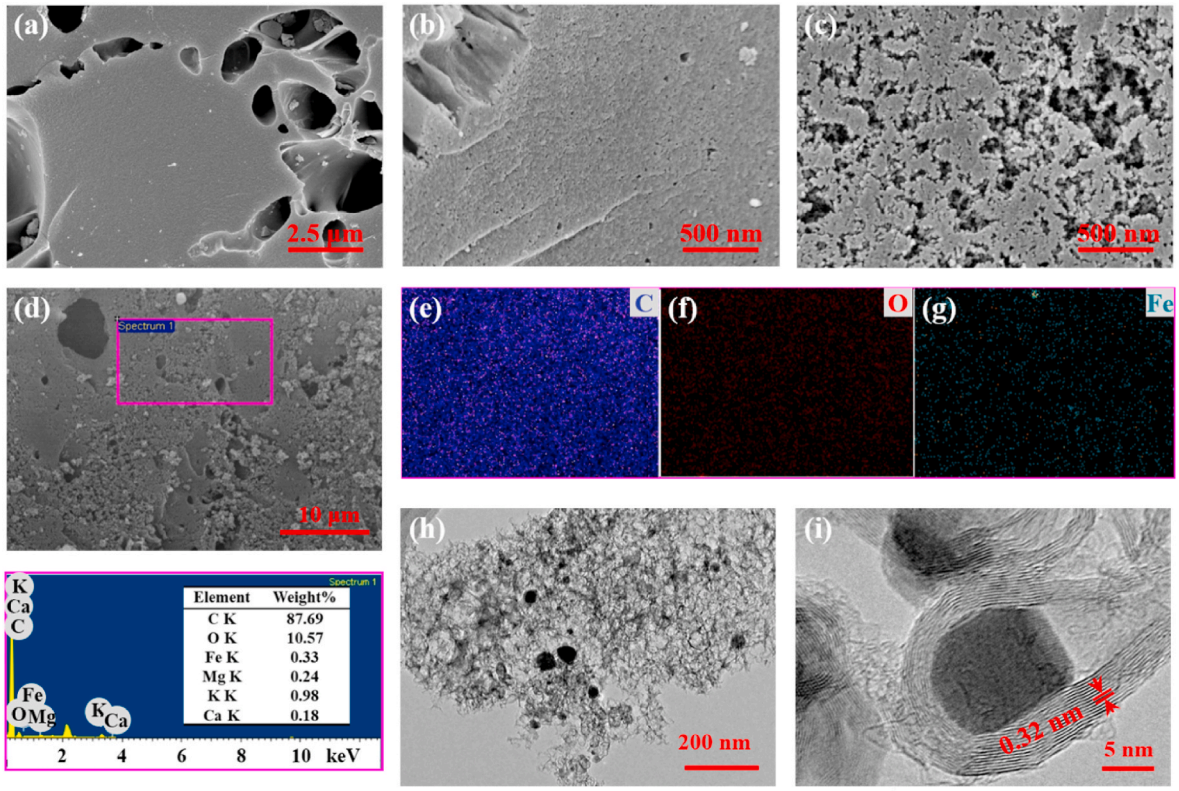

Fig. 2. SEM and TEM views of as-synthesized materials. SEM images of (a) raw carbonized coconut shell, (b) AC, and (c) NZVI@MAC. (d–g) EDS spectra and element mapping and (h, i) TEM images of NZVI@MAC.

of 1.21 m^3 g^{-1}, which was used for the following adsorption experiments. The control sample without Fe^0 was named as AC.

3.2. Characterizations of NZVI@MAC

The structure, morphology, composition and property of NZVI@MAC was investigated. The NZVI@MAC exhibited a representative pattern of IV type adsorption-desorption with a hysteresis loop revealing the existence of mesoporous (Fig. 1d). It possessed a wide range of pore size distribution with abundant micropore and mesoporous in sharp contrast to AC (Fig. 1e). The micro-characteristics of samples were illustrated in Fig. 2. Some macropores were observed on the carbonized material by SEM (Fig. 2a). After activation, its relatively smooth surface was transformed into porous structures, especially for NZVI@MAC (Fig. 2b and c). The characteristic of gradient pore (macro-, meso- and micro-pore) of the NZVI@MAC could be identified, which was quite beneficial for the adsorption of pollutants with different sizes. Element mapping confirmed that the elements of C, O and Fe were dispersed uniformly (Fig. 2e–g). The in-situ synthesized NZVI (merely 0.33 wt%) (Fig. 2d) exhibited a strikingly positive effect on pore formation and expansion. The spherical NZVI particles with an approximate size range of 20–50 nm were firmly embedded and encapsulated in the carbon carrier (Fig. 2h and i). These phenomena demonstrated that the Fe^{3+}, underwent the process of carbothermal reduction coupled with catalytic activation, had nucleated successfully and grown into NZVI particles and dispersed uniformly in MAC frameworks (Wu et al., 2019), which showed a striking contrast to the chain-like NZVI particles formed by liquid phase reduction on AC surfaces (Liu et al., 2019). The lattice fringe spacing (approximate 0.32 nm) around the NZVI was identified to the (002) lattice plane of graphite carbon, which implied that the NZVI might also catalyze the amorphous carbon to form hydrophobic graphitic layers covering its surface. By contrast, no similar structure in AC could be found. These consequents could also be proven by the water contact angle measurements (Fig. 3b). The hydrophobic NZVI@MAC particles became more hydrophilic after grinding because the surface structure was destroyed. This graphitic structure on the surface of NZVI@MAC significantly enhanced its hydrophobicity, and increased the affinity for efficiently removing organic pollutants.

Raman spectroscopy was used to characterize the degree of lattice defect (Fig. 1f). The I_D/I_G value of the NZVI@MAC (1.18) was higher than that of AC (1.03), indicating that the doping of NZVI increased the defective degree of material in associated with the formation of the mesoporous morphology. The forming process, structure of NZVI@MAC was shown in Fig. 3a.

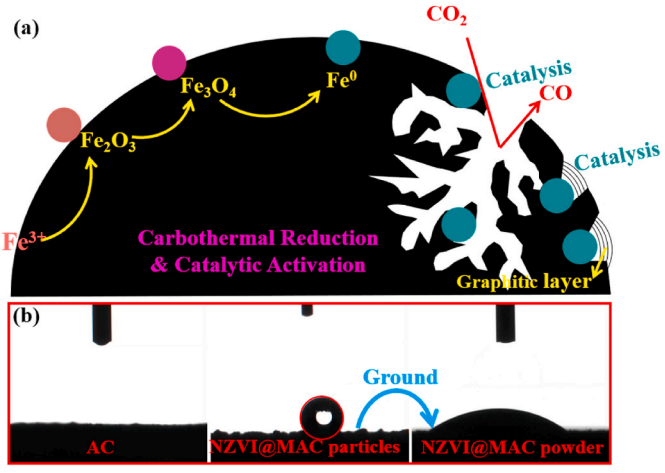

Fig. 3. (a) Schematic illustration of NZVI@MAC. (b) Water contact angles of NZVI@MAC and AC.

3.3. BPA adsorption performance

3.3.1. Effects of material synthesis conditions

The effects of material synthesis conditions on BPA adsorption were investigated (Fig. S2). The NZVI@MAC prepared with 0.25 wt% Fe^{3+} exhibited excellent adsorption capacity and efficiency for BPA compared with the AC, which demonstrated that the modification of AC with an appropriate dosage of Fe^{3+} could promote its adsorption performance. The NZVI@MAC prepared using water/alcohol solution (v: v = 4: 1) as dispersant also exhibited a higher adsorption performance. This mixture containing 90% ethanol was employed to disperse the NZVI particles synthesized by liquid phase reduction (Wang et al., 2009). But in this study, the increased ethanol proportion caused the decline in the specific surface area of adsorbents as well as their adsorption capacity for BPA, which demonstrated that excessive ethanol was related to the poor dispersion of NZVI. In addition, a larger specific surface area of NZVI@MAC was achieved at 850 °C for 100 min or with 0.6 L min^{-1} of CO_2, which resulted in the great adsorption capacity of BPA.

3.3.2. Adsorption kinetics, isotherms and thermodynamics

Kinetics models (Pseudo-first-order, Pseudo-second-order and Elovich model) were exploited to analyze the adsorption data (Fig. 4a, Table S2). The higher correlation coefficients (R^2) and the closer values of q_e^{cal} to qe^{exp} indicated that the Pseudo-second-order models were more suitable for the experimental data of BPA adsorption on NZVI@MAC (R^2 = 0.9930). However, the adsorption on AC followed the Elovich model (R^2 = 0.9708). The initial adsorption rate (h) of BPA on the NZVI@MAC was nearly 8.62 times faster than that on AC. Liquid film diffusion and Intra-particle diffusion models were used to investigate the rate-limiting step (Fig. 4b and c, Table S3). The results showed that the liquid film diffusion was the main rate-controlling step for the BPA adsorption on AC (R^2 = 0.9903). The Intra-particle diffusion could be divided into two stages with R^2 of 0.9489–0.9937. Both of the fitted trendlines did not pass through the origin, demonstrating that the adsorption rates were affected not only by the inner diffusion but also by other processes. In the first stage, the exterior diffusion from the solution to the adsorbent surface might be the main speed limiting step, where the BPA adsorption onto NZVI@MAC owned significantly higher rate constant (91.29 mg g^{-1} $h^{-0.5}$) than that onto AC (27.16 mg g^{-1} $h^{-0.5}$). In the second part, Intra-particle diffusion became the main influence factor.

The forms of BPA adsorption at different temperatures were further analyzed using isotherm models (Langmuir, Freundlich, Temkin and Dubinin-Radushkevich model, Fig. 4d–f, Table S4). By contrast, the Langmuir model showed higher R^2 (>0.9872) on NZVI@MAC and AC, suggesting that homogeneous monolayer adsorption might primarily occur on the surface. The lower values of R_L (<1) meant that the adsorption processes of BPA were favorable, and the higher values of K_L (0.11–0.13) manifested that the adsorption energies on NZVI@MAC were much higher than that on AC (Meena et al., 2005). However, relatively high R^2 (>0.9807) of Freundlich models for AC indicated that the energy distribution on the real solid surfaces was not quite uniform. The high values of 1/n (<1) also suggested that the degree of surface heterogeneity of plain AC was much higher than that of NZVI@MAC, and the adsorption was favorable and associated with a physical process (Vimonses et al., 2009). The modification of NZVI on AC changed the adsorption behavior of BPA. Furthermore, the adsorption data were also fitted well with Temkin models (R^2 > 0.9842), revealing that the BPA adsorption on both adsorbents was exothermic (b_T > 1) based on the assumption of this model. The above consequents showed that BPA adsorption on both adsorbents might be dominated as a chemical and physical adsorption process. The fitted adsorption capacities (q_m) of BPA on NZVI@MAC and AC were 327.60 and 322.66 mg g^{-1}, respectively, demonstrating that the NZVI@MAC could slightly increase the adsorption of BPA even the pore expansion and occupation of NZVI particles reduced its specific surface area. Compared with other mesoporous materials (Table 2), the maximum adsorption capacity of NZVI@MAC

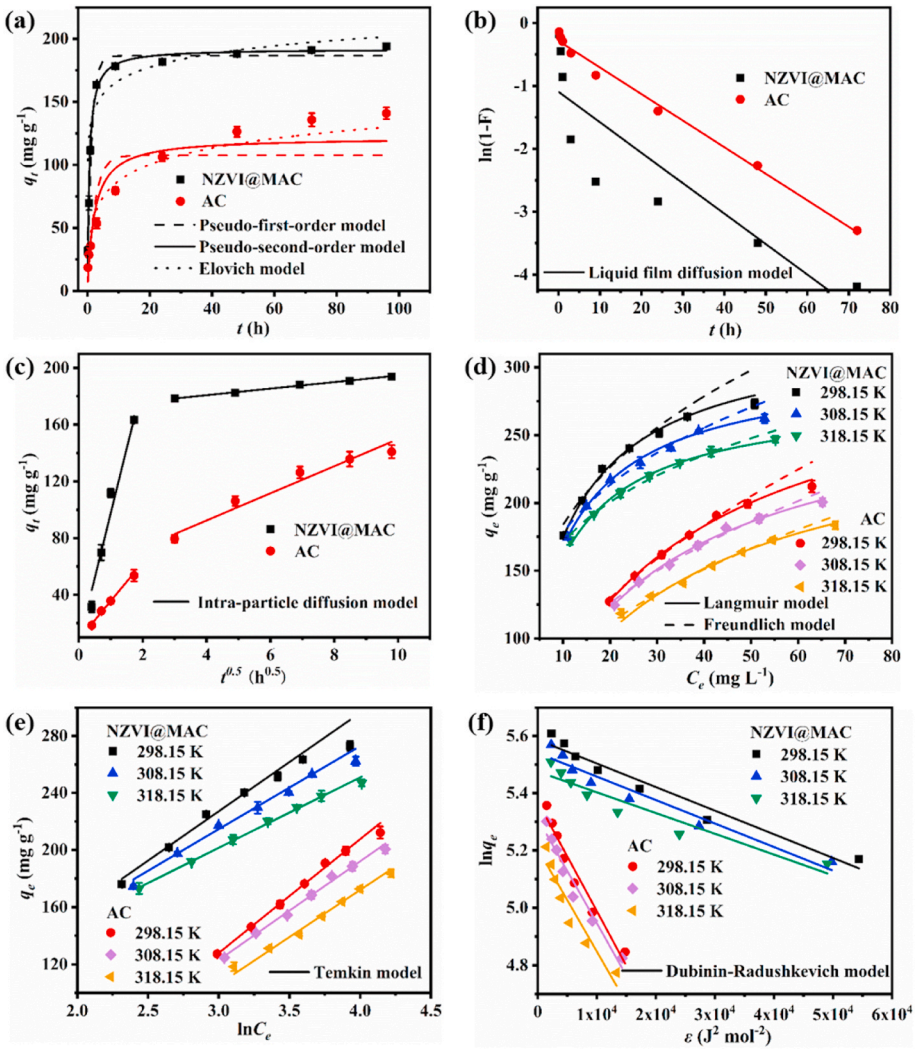

Fig. 4. Fitting models of BPA adsorption on NZVI@MAC and AC. (a) Kinetic models, (b) Liquid film diffusion models, (c) Intra-particle diffusion models, (d) Langmuir and Freundlich models, (e) Temkin models and (f) Dubinin-Radushkevich models of NZVI@MAC and AC.

Table 2
Summary of various adsorbents for BPA removal.

Adsorbents	modification method	Isotherm models	q_m (mg g^{-1})	References
AC	H_3PO_4	L	220	(Hernández-Abreu et al., 2021)
Powers AC	Chitosan-polyvinyl alcohol	L	64.6	Zhou et al. (2020)
Powers AC		L	290	Libbrecht Wannes (2015)
OMC	Hard templated	L	474	Libbrecht Wannes (2015)
OMC	Soft templated	L	154	Libbrecht Wannes (2015)
OMC	Hard templated	L	296	Sui et al. (2011)
Fe/OMC	Nano iron	F	311	Tang et al. (2016)
Mesoporous carbonized material	HF	L	103.32	Wan et al. (2021)
NZVI@MAC	NZVI	L	327.60	This study

was among the highest values of mesoporous carbon materials. Besides, the hydrophobic NZVI@MAC synthesized by a simple, cost-effective, sustainable, eco-friendly process showed promising potential for mass production and practical applications especially in drinking water purification.

From the isotherm models (Table S5), the thermodynamic parameters of negative values of ΔG (−20-0 kJ mol^{-1}), ΔH *and* ΔS disclosed that the BPA adsorption was a spontaneous, exothermic physical adsorption process, and the adsorption system tended to be stable (Vimonses et al., 2009). The value of $|\Delta G|$ of each adsorbent was decreased with the increased temperature, consisted with the decrease of the adsorption capacity at high temperatures. Under the same temperature, the value of $|\Delta G|$ of NZVI@MAC was always larger than that of AC demonstrating that NZVI@MAC was more favorable for BPA adsorption.

3.3.3. *Relationships between adsorption performance and pore structure*

The relationships between the adsorption performance of BPA and the pore structure of adsorbents were analyzed statistically (Fig. 5a–d). The adsorption capacities and initial adsorption rates were positively correlated with the total specific surface area (Pearson's r = 0.9367) as well as the mesoporous specific surface area (Pearson's r = 0.9152). However, the further analyses illustrated that the initial adsorption rates were slow when the average pore size was less than 4.0 nm or the mesoporous proportion was lower than 70%. That was, the effective active sites for BPA adsorption on the inner surface of MAC were increased while the pore size was large enough to accommodate BPA, then BPA with lower diffusion resistance could quickly arrive at the

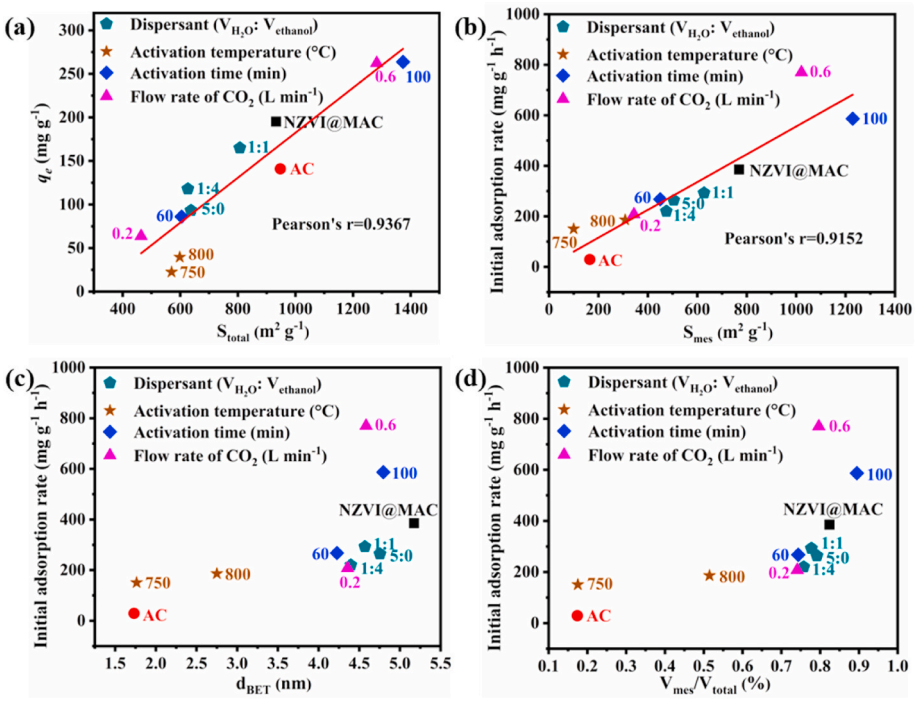

Fig. 5. Relationships between the adsorption performance of BPA and the pore structure of adsorbents. (a) Correlations between the S_{total} of adsorbents and their adsorption capacity for BPA, (b) S_{mes}, (c) d_{BET}, (d) V_{meso}/V_{total} of the adsorbents and the initial adsorption rate. More detailed information of the adsorbents can be seen in Table S1.

active sites. Therefore, the adsorption efficiency and capacity of BPA could be enhanced by appropriately increased mesoporous proportion (70–90%) with enlarged average pore size (4.1–5.2 nm). In addition, further investigations were employed to illuminate the interaction mechanisms between BPA and NZVI@MAC.

3.4. Effects of external environmental factors

The effects of initial pH and coexisting ions on BPA adsorption by NZVI@MAC and AC were explored respectively (Fig. 6a–c). The point of zero charge of both adsorbents was similar (at pH ≈ 2.3), and their

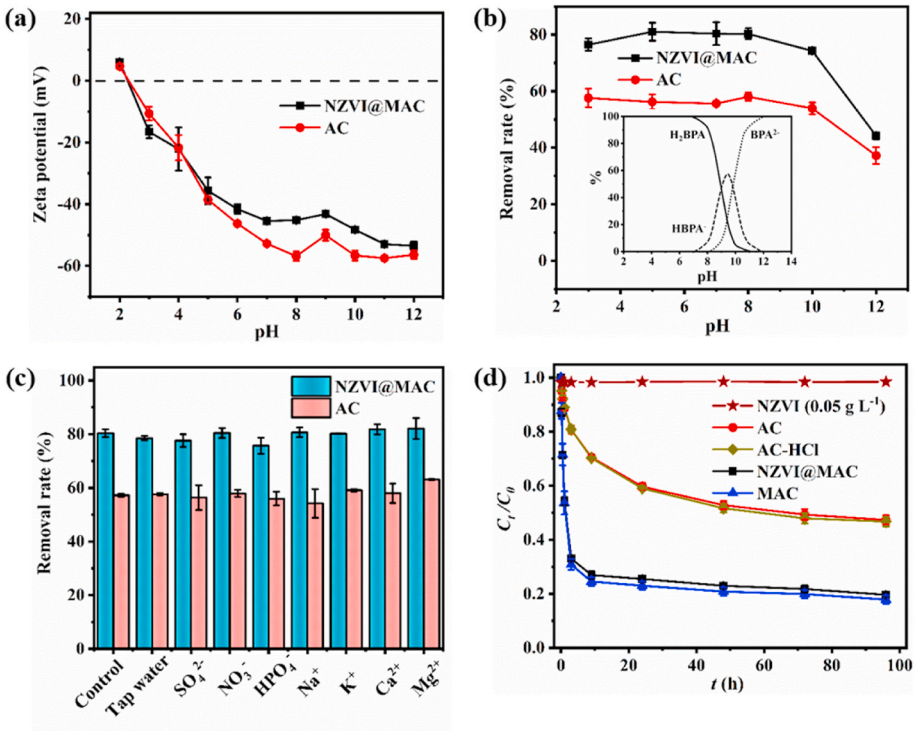

Fig. 6. Effects of environmental conditions and NZVI on BPA adsorption. (a) Zeta potential analysis of NZVI@MAC and AC. Comparison of the effects of (b) initial pH and (c) coexisting ions (0.1 M) on the BPA adsorption performances of NZVI@MAC and AC. The insert of (b) is the p*K*a of BPA. (d) BPA removal efficiency of different adsorbents. Pickling conditions: impregnated with 10% boiling HCl for 2 h, followed by a rinsing process with water until the pH of supernatant become neutral.

variation trends of zeta potential were the same (Fig. 6a). These results suggested that the modification of small amount of NZVI (0.33%) would hardly influence the zeta potential of NZVI@MAC. When the pH of solution was higher than 2.3, the surface charge of both adsorbents was negative. For BPA (p*Ka* = 9.6/10.2) (Toledo et al., 2005), when the pH is higher than 8.0, the increased electrostatic repulsion between the negatively charged adsorbent and anionic species ($HBPA^-$ and BPA^{2-}) causes a prominent decline in the BPA adsorption. However, both adsorbents could maintain high adsorption performance in a wide pH range of 3–10 (Fig. 6b). The interference of coexisting inorganic ions (SO_4^{2-}, NO_3^-, HPO_4^{2-}, Na^+, K^+, Ca^{2+} and Mg^{2+}) on BPA adsorption was also investigated (Fig. 6c). The removal rates of BPA on both materials were hardly affected by coexisting ions and in tap water. These results unclosed the excellent anti-interference performance of NZVI@MAC and AC.

4. Adsorption mechanism verification

To investigate the effect of NZVI on BPA adsorption, different adsorbents were prepared and compared (Fig. 6d). NZVI, with a higher adding amount than the content of NZVI in NZVI@MAC, showed a negligible adsorption capacity on BPA. Furthermore, the comparison of NZVI@MAC and MAC (NZVI was completely removed by HCl and confirmed by EDS mapping in Fig. S3) was further conducted to directly investigate the role of NZVI in the efficiency of BPA adsorption. The impact of pickling on carbon skeleton could be ignored because the adsorption performance of AC and HCl-treated AC was almost the same. The normalized adsorption capacities (adsorption capacity divided by specific surface area, q_N) of NZVI@MAC and MAC were similar at 0.21 mg m^{-2}, indicating that the NZVI showed neither positive nor negative effect on the BPA adsorption process. However, the q_N of NZVI@MAC was higher than that of AC (0.15 mg m^{-2}) and the initial adsorption rate of former was 8.67-fold higher. Thus, it should be specifically emphasized that, although the interaction between NZVI and BPA could be ignored, the greatly improved adsorption rate and capability were mainly attributed to the role of NZVI in constructing the rich mesoporous structure and hydrophobic property.

Generally, π-π interaction, hydrophobic effect, electrostatic interaction and hydrogen bonding are the main interactions between carbonaceous materials and aromatic compounds. Among them, π-π interaction commonly plays a leading role. The strong adsorption affinity is based on the π-donor with π-electron-rich regions on sp^2 hybridized carbon and the π-acceptor with π-electron-depleted property of BPA (Sun et al., 2020). The higher the graphitization degree of the carbonaceous materials is, the stronger the driving force for BPA adsorption via π-π interaction becomes. Our results confirmed that the adsorption capacity of BPA on NZVI@MAC with more graphitic defects was higher than that of on AC. The adsorption capacities on NZVI@MACs presented a positive correlation (Pearson's r = 0.8862) to the degree of graphitic defects represented by the I_D/I_G value (Fig. 7a).

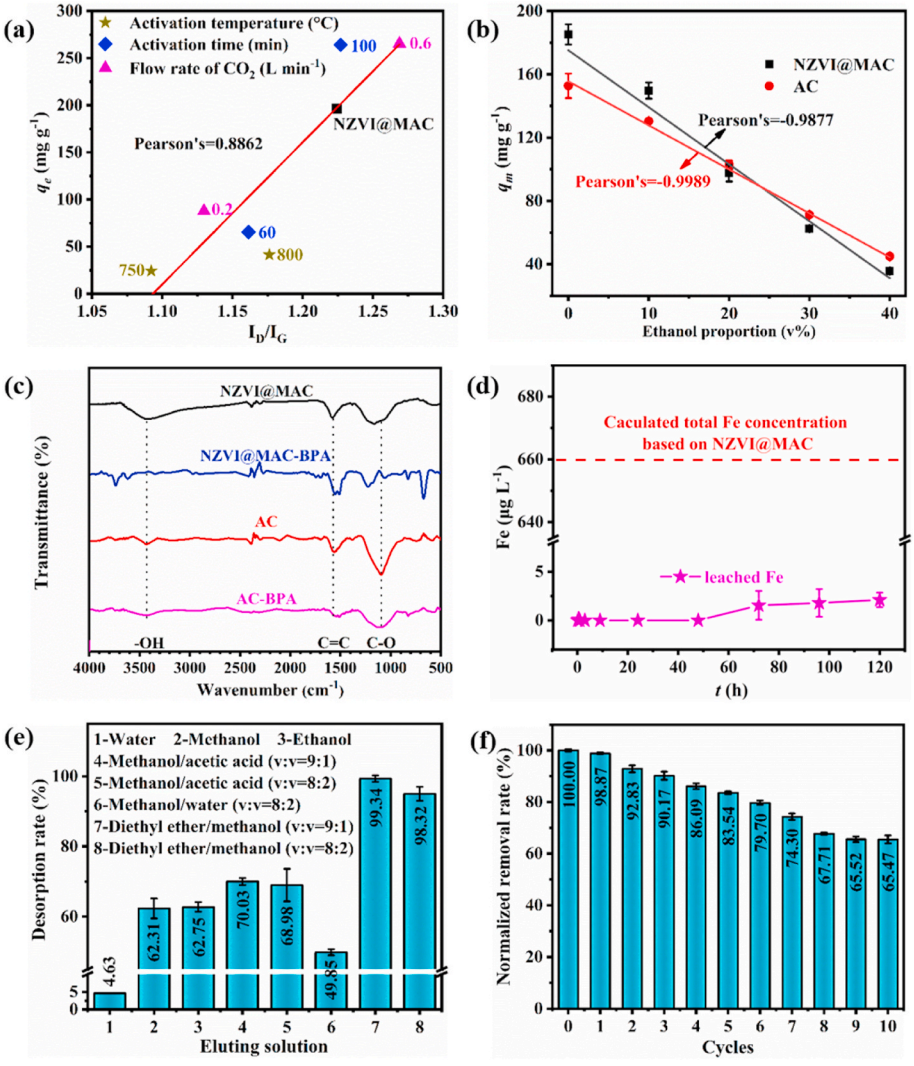

Fig. 7. (a) Correlations between the I_D/I_G values of adsorbents and their adsorption capacities for BPA, and more detailed information of the adsorbents can be seen in Table S1. (b) Correlations between the ethanol proportion in solution and the adsorption capacities of BPA on NZVI@MAC and AC. (c) FTIR spectra of pristine and saturated NZVI@MAC and AC. (d) The concentration of leached Fe from NZVI@MAC in water. (e) Effects of organic solvents on BPA desorption from the saturated NZVI@MAC. (f) Regeneration performance of NZVI@MAC.

These phenomena revealed that π-π interaction between BPA and NZVI@MAC was not the dominant mechanism.

Hydrophobic interaction is of great importance for the adsorption of hydrophobic pollutants ($\log K_{ow}$ of BPA = 3.32) (Lei et al., 2013). Ethanol could weaken the interaction between carbonaceous materials and organic adsorbents (Lambrecht et al., 2016), therefore BPA adsorption in a different volume ratio of ethanol/water solution was investigated. The adsorption capacity of BPA on NZVI@MAC and AC manifested negative linear relationships (Pearson's r > 0.98) with the ethanol proportion increased from 0 to 40% (Fig. 7b), and the absolute value of slope on NZVI@MAC was larger than that of on AC, indicating that the hydrophobicity of NZVI@MAC was greater. For a more hydrophobic organic pollutant, triclosan ($\log K_{ow}$ = 4.76, 0.69 × 0.75 × 1.42 nm^3), its adsorption on NZVI@MAC and AC displayed similar trends with higher removal performance with respect to BPA (Fig. S4). This observation confirmed that the BPA adsorption on NZVI@MAC was driven robustly by hydrophobic interaction and the NZVI@MAC was a broad-spectrum adsorbent for effective removal of bulky hydrophobic organic pollutants. Hydrophobic interaction can not only affect the adsorption of hydrophobic pollutants in a longer range but also lead to the initial stage of adsorption (Xie et al., 2020). Additionally, this interaction is less likely to be affected by the interference of the co-existing salt (Stock et al., 2015).

Electrostatic interaction between neutral BPA and adsorbent could be neglected at pH below 8.0. Hydrogen bonds are likely to form between the hydrogen atoms in the hydroxyl group of BPA and the highly electronegative atoms (*e.g.*, N, O, and F) on the surface of the adsorbent. FTIR was used to characterize the surface functional groups of the pristine and saturated samples (Fig. 7c). The bands in the range of 3100–3700 cm^{-1} (–OH), 1400-1700 cm^{-1} (C=C) and 900–1300 cm^{-1} (C–O) (Arampatzidou and Deliyanni, 2016) were all characteristic bands of the carbonaceous materials. The new peaks at 823 cm^{-1} and 674 cm^{-1} on the saturated adsorbents was associated with the BPA adsorption. Besides, the shift of the C–O stretching band might correspond to the formation of hydrogen bonds, while the slight shift of the C=C stretching vibration band might be related to the π-π interactions. However, the disappearance of the peaks near 3400 cm^{-1} signified that the hydrogen bonds had not formed after the BPA adsorption. The original –OH groups might be contributed from the chemisorbed water in the air.

Furthermore, the interface interactions between the adsorbate and adsorbent can be easily affected by solution pH. The increase of solution pH (>8.0) could weaken the hydrogen bonding because the ionized BPA could not provide the proton on the hydroxyl to form hydrogen bonds. It can also enhance the electrostatic repulsion between the negatively charged adsorbents and the anionic BPA. Meanwhile, hydrophobic interaction could also be decreased due to the increased hydrophilicity of the ionized BPA. Finally, the increase of pH could increase the π-π interaction by promoting π-electron-donor ability of the sp^2 hybridized carbon of the adsorbent (Pan and Xing, 2008; Zhang et al., 2010). The slight decline of the removal rate of BPA on both adsorbents in the pH range of 3.0–10.0 (Fig. 6b) indicated that hydrogen bonding might play a minor role. However, the sharply decreased removal rate in the pH range of 10.0–12.0 implied that the increased π-π interaction could not counteract the increased electrostatic repulsion, the decreased hydrophobic interaction and hydrogen bonding. In contrast, the smaller gap of the removal rate (pH = 3–12) on AC signified that the stronger π-π interaction could neutralize more negative interaction. In short, for ionizable BPA, its adsorption mechanisms could be affected by environment conditions. Under neutral conditions, the high adsorption performance of BPA on NZVI@MAC was primarily attributed to the strong hydrophobic interaction, π-π interaction and weak hydrogen bonding (Fig. 8).

The concentrations of leaching Fe from NZVI@MAC were detected (Fig. 7d). The maximum concentration of leaching Fe was only 2.11 μg L^{-1} in water for 120 h and accounted for merely 0.32% of the theoretical value of Fe in NZVI@MAC, indicating that the structure of NZVI@MAC was extremely stable and safe for drinking water purification. In sharp contrast to the effect of pH on BPA desorption (21.39% at pH = 12.0, Fig. S5), the organic solvents performed excellent elution effects (Fig. 7e). The desorption rate in the methanol/acetic acid mixture was higher than in methanol as more hydrogen bonds were ruptured (Xu et al., 2011). Ethanol was reported to have a high desorption efficiency for BPA bounded by hydrophobic interaction (Shao et al., 2021). But in this work, only 62.75% of BPA was desorbed, suggesting that multiple interactions might be involved in the adsorption. The diethyl ether/-methanol mixture (v: v = 9: 1) displayed the best desorption rate of 99.34%, proving that the mixture could facilitate breaking the multiple interactions between BPA and NZVI@MAC. After eluting with the diethyl ether/methanol mixture, the adsorption capacity of BPA on

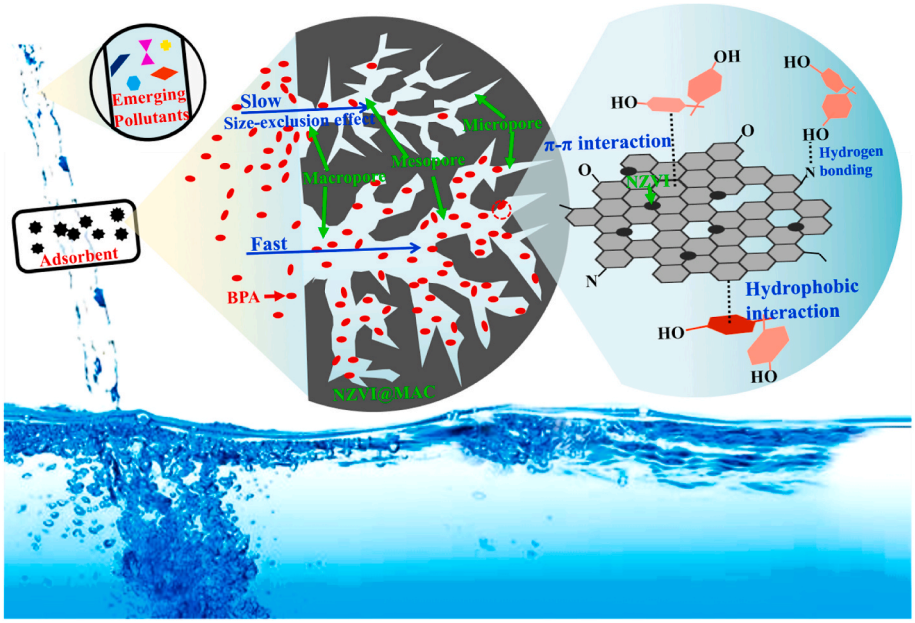

Fig. 8. Proposed mechanism of BPA adsorption on NZVI@MAC.

NZVI@MAC gradually decreased, but it still kept 83.54% of original value after 5 cycles. In addition, the decrement rate of adsorption capacity tended to be stable after 7 cycles, and the removal rate decreased by 34.52% after 10 cycles, remaining at about 65% of the original adsorption capacity (Fig. 7f). The results suggested that the NZVI@MAC was a structural stable, safe, well regenerative and economic adsorbent.

5. Conclusions

In this study, a novel one-step approach by coupling carbothermal reduction with catalytic activation was firstly proposed to facilely prepare the hydrophobic NZVI@MAC using sustainable carbonized coconut shell impregnated with Fe^{3+} as precursor and CO_2 as activator. The in-situ synthesized NZVI (merely 0.33 wt%) by carbothermal reduction could catalyze the gasification reaction between carbon and CO_2 to fabricate the MAC, the dispersive NZVI but also catalyze the amorphous carbon to form hydrophobic graphitic layers on its surface. The NZVI@MAC possessed not only a high mesoporous proportion (82.41%) with a gradient pore structure ($D_{BET} = 5.17$ nm), but also a large specific surface area (933.12 $m^2\ g^{-1}$) and total pore volume (1.21 $m^3\ g^{-1}$). Further researches disclosed that the hydrophobic NZVI@MAC dramatically improved the initial adsorption rate by 8.62-fold with a slightly increased adsorption capacity of 327.60 mg g^{-1} for BPA with respect to the unmodified AC. The pore size (4.1–5.2 nm) of NZVI@MAC with high mesoporous proportion (70–90%) facilitated the rapid adsorption of BPA with lower diffusion resistance. The adsorption mechanism involved strong hydrophobic interaction, π-π interaction and weak hydrogen bonding under neutral conditions. On these grounds, the NZVI@MAC still showed high adsorption performance in a wide pH range (pH = 3–10) and in the presence of different inorganic ions. Furthermore, the structural stable NZVI@MAC granule can be easily separated and regenerated maintaining a 65.47% removal rate after 10 cycles. Therefore, the hydrophobic NZVI@MAC synthesized using a simple, robust, economic, eco-friendly and easy scale-up procedure exhibited a great potential for practical applications even for drinking water purification.

CRediT authorship contribution statement

Qingxin Xu: Conceptualization, Methodology, Formal analysis, Investigation, Resources, Data curation, Writing – original draft, Writing – review & editing, Visualization. **Xuejiao Liu:** Investigation, Funding acquisition. **Dengguo Lai:** Methodology, Writing – review & editing, Visualization, Funding acquisition. **Zhenjiao Xing:** Investigation, Resources. **Pamphile Ndagijimana:** Investigation, Data curation. **Zhiwei Li:** Investigation, Data curation. **Yin Wang:** Funding acquisition, Project administration, Validation, Supervision, Writing – review & editing.

Declaration of competing interest

The authors declare that they have no known competing financial interests or personal relationships that could have appeared to influence the work reported in this paper.

Acknowledgments

The research was financially supported by the Special Research Assistant Program of the Chinese Academy of Sciences, the Strategic Priority Research Program of the Chinese Academy of Sciences (No. XDA23030301), the Industry Leading Key Projects of Fujian Province (No. 2019H0056), the Social Development Leading Key Projects of Fujian Province (No. 2021Y0069).

Appendix A. Supplementary data

Supplementary data to this article can be found online at https://doi.org/10.1016/j.jclepro.2022.131854.

References

Arampatzidou, A.C., Deliyanni, E.A., 2016. Comparison of activation media and pyrolysis temperature for activated carbons development by pyrolysis of potato peels for effective adsorption of endocrine disruptor bisphenol-A. J. Colloid Interface Sci. 466, 101–112. https://doi.org/10.1016/j.jcis.2015.12.003.

Careghini, A., Mastorgio, A.F., Saponaro, S., Sezenna, E., 2015. Bisphenol A, nonylphenols, benzophenones, and benzotriazoles in soils, groundwater, surface water, sediments, and food: a review. Environ. Sci. Pollut. Res. 22, 5711–5741. https://doi.org/10.1007/s11356-014-3974-5.

Dai, Y., Hu, Y., Jiang, B., Zou, J., Tian, G., Fu, H., 2016. Carbothermal synthesis of ordered mesoporous carbon-supported nano zero-valent iron with enhanced stability and activity for hexavalent chromium reduction. J. Hazard Mater. 309, 249–258. https://doi.org/10.1016/j.jhazmat.2015.04.013.

Dong, Y., Lin, H., Qu, F., 2012. Synthesis of ferromagnetic ordered mesoporous carbons for bulky dye molecules adsorption. Chem. Eng. J. 193–194, 169–177. https://doi.org/10.1016/j.cej.2012.04.024.

Flint, S., Markle, T., Thompson, S., Wallace, E., 2012. Bisphenol A exposure, effects, and policy: a wildlife perspective. J. Environ. Manag. 104, 19–34. https://doi.org/10.1016/j.jenvman.2012.03.021.

Hadoun, H., Sadaoui, Z., Souami, N., Sahel, D., Toumert, I., 2013. Characterization of mesoporous carbon prepared from date stems by H_3PO_4 chemical activation. Appl. Surf. Sci. 280, 1–7. https://doi.org/10.1016/j.apsusc.2013.04.054.

He, Y., Gao, J.F., Feng, F.Q., Liu, C., Peng, Y.Z., Wang, S.Y., 2012. The comparative study on the rapid decolorization of azo, anthraquinone and triphenylmethane dyes by zero-valent iron. Chem. Eng. J. 179, 8–18. https://doi.org/10.1016/j.cej.2011.05.107.

Hernández-Abreu, A.B., Álvarez-Torrellas, S., Rocha, R.P., Pereira, M.F.R., Águeda, V.I., Delgado, J.A., Larriba, M., García, J., Figueiredo, J.L., 2021. Effective adsorption of the endocrine disruptor compound bisphenol a from water on surface-modified carbon materials. Appl. Surf. Sci. 552 https://doi.org/10.1016/j.apsusc.2021.149513.

Hoch, L.B., Mack, E.J., Hydutsky, B.W., Hershman, J.M., Skluzacek, J.M., Mallouk, T.E., 2008. Carbothermal synthesis of carbon-supported nanoscale zero-valent iron particles for the remediation of hexavalent chromium. Environ. Sci. Technol. 42, 2600–2605. https://doi.org/10.1021/es702589u.

Hong, E.H., Jung, Y.H., Lee, K.H., 2000. Preparation of mesoporous activated carbon fibers by catalytic gasification. Kor. J. Chem. Eng. 17, 237–240. https://doi.org/10.1007/BF02707149.

Hu, Z., Srinivasan, M.P., 2001. Mesoporous high-surface-area activated carbon. Microporous Mesoporous Mater. 43, 267–275. https://doi.org/10.1016/S1387-1811(00)00355-3.

Jeirani, Z., Niu, C.H., Soltan, J., 2017. Adsorption of emerging pollutants on activated carbon. Rev. Chem. Eng. 33, 1–32. https://doi.org/10.1515/revce-2016-0027.

Ji, L., Liu, F., Xu, Z., Zheng, S., Zhu, D., 2010. Adsorption of pharmaceutical antibiotics on template-synthesized ordered micro- and mesoporous carbons. Environ. Sci. Technol. 44, 3116–3122. https://doi.org/10.1021/es903716s.

Jiang, S.F., Ling, L.L., Chen, W.J., Liu, W.J., Li, D.C., Jiang, H., 2019. High efficient removal of bisphenol A in a peroxymonosulfate/iron functionalized biochar system: mechanistic elucidation and quantification of the contributors. Chem. Eng. J. 359, 572–583. https://doi.org/10.1016/j.cej.2018.11.124.

Kang, J.H., Kondo, F., Katayama, Y., 2006. Human exposure to bisphenol A. Toxicology 226, 79–89. https://doi.org/10.1016/j.tox.2006.06.009.

Kaur, H., Hippargi, G., Pophali, G.R., Bansiwal, A., 2019. Biomimetic lipophilic activated carbon for enhanced removal of triclosan from water. J. Colloid Interface Sci. 535, 111–121. https://doi.org/10.1016/j.jcis.2018.09.093.

Lambrecht, M.A., Rombouts, I., Delcour, J.A., 2016. Denaturation and covalent network formation of wheat gluten, globular proteins and mixtures thereof in aqueous ethanol and water. Food Hydrocolloids 57, 122–131. https://doi.org/10.1016/j.foodhyd.2016.01.018.

Lei, C., Hu, Y., He, M., 2013. Adsorption characteristics of triclosan from aqueous solution onto cetylpyridinium bromide (CPB) modified zeolites. Chem. Eng. J. 219, 361–370. https://doi.org/10.1016/j.cej.2012.12.099.

Li, X., Zhang, L., Yang, Z., He, Z., Wang, P., Yan, Y., Ran, J., 2020. Hydrophobic modified activated carbon using PDMS for the adsorption of VOCs in humid condition. Separ. Purif. Technol. 239 https://doi.org/10.1016/j.seppur.2020.116517.

Lian, Q., Yao, L., Ahmad, Z.U., Gang, D.D., Konggidinata, M.l., Gallo, A.A., Zappi, M.E., 2020. Enhanced Pb(II) adsorption onto functionalized ordered mesoporous carbon (OMC) from aqueous solutions: the important role of surface property and adsorption mechanism. Environ. Sci. Pollut. Res. 27, 23616–23630. https://doi.org/10.1007/s11356-020-08487-9.

Libbrecht Wannes, V.K., De Buysser, Klaartje, Verberckmoes, An, Thybaut, Joris, Poelman, Hilde, De Clercq, Jeriffa, Der Voort, Pascal Van, 2015. Tuning the pore geometry of ordered mesoporous carbons for enhanced adsorption of bisphenol-A. Materials 8, 1652–1665. https://doi.org/10.3390/ma8041652.

Liew, R.K., Azwar, E., Yek, P.N.Y., Lim, X.Y., Cheng, C.K., Ng, J.H., Jusoh, A., Lam, W.H., Ibrahim, M.D., Ma, N.L., Lam, S.S., 2018. Microwave pyrolysis with KOH/NaOH mixture activation: a new approach to produce micro-mesoporous activated carbon for textile dye adsorption. Bioresour. Technol. 266, 1–10. https://doi.org/10.1016/j.biortech.2018.06.051.

Liu, X., Lai, D., Wang, Y., 2019. Performance of Pb(II) removal by an activated carbon supported nanoscale zero-valent iron composite at ultralow iron content. J. Hazard Mater. 361, 37–48. https://doi.org/10.1016/j.jhazmat.2018.08.082.

Liu, Z., Ling, L., Qiao, W., Liu, L., 1999. Preparation of pitch-based spherical activated carbon with developed mesopore by the aid of ferrocene. Carbon 37, 663–667. https://doi.org/10.1016/S0008-6223(98)00242-5.

Magalhães, F., Pereira, M.C., Fabris, J.D., Bottrel, S.E.C., Sansiviero, M.T.C., Amaya, A., Tancredi, N., Lago, R.M., 2009. Novel highly reactive and regenerable carbon/iron composites prepared from tar and hematite for the reduction of Cr(VI) contaminant. J. Hazard Mater. 165, 1016–1022. https://doi.org/10.1016/j.jhazmat.2008.10.087.

Meena, A.K., Mishra, G.K., Rai, P.K., Rajagopal, C., Nagar, P.N., 2005. Removal of heavy metal ions from aqueous solutions using carbon aerogel as an adsorbent. J. Hazard Mater. 122, 161–170. https://doi.org/10.1016/j.jhazmat.2005.03.024.

Oh, S.Y., Seo, Y.D., Ryu, K.S., Park, D.J., Lee, S.H., 2017. Redox and catalytic properties of biochar-coated zero-valent iron for the removal of nitro explosives and halogenated phenols. Environ. Sci.: Process. Impacts 19, 711–719. https://doi.org/10.1039/C7EM00035A.

Padhye, L.P., Yao, H., Kung`u, F.T., Huang, C.H., 2014. Year-long evaluation on the occurrence and fate of pharmaceuticals, personal care products, and endocrine disrupting chemicals in an urban drinking water treatment plant. Water Res. 51, 266–276. https://doi.org/10.1016/j.watres.2013.10.070.

Pan, B., Xing, B., 2008. Adsorption mechanisms of organic chemicals on carbon nanotubes. Environ. Sci. Technol. 42, 9005. https://doi.org/10.1021/es801777n.

Peng, X., Hu, F., Lam, F.L.-Y., Wang, Y., Liu, Z., Dai, H., 2015. Adsorption behavior and mechanisms of ciprofloxacin from aqueous solution by ordered mesoporous carbon and bamboo-based carbon. J. Colloid Interface Sci. 460, 349–360. https://doi.org/10.1016/j.jcis.2015.08.050.

Qiao, W., Song, Y., Yoon, S.H., Mochida, I., 2005. Modification of commercial activated carbon through gasification by impregnated metal salts to develop mesoporous structures. N. Carbon Mater. 20, 198–204. https://doi.org/10.3321/j.issn:1007-8827.2005.03.002.

Rahman, A., Hango, H.J., Daniel, L.S., Uahengo, V., Jaime, S.J., Bhaskaruni, S.V.H.S., Jonnalagadda, S.B., 2019. Chemical preparation of activated carbon from Acacia erioloba seed pods using H_2SO_4 as impregnating agent for water treatment: an environmentally benevolent approach. J. Clean. Prod. 237, 117689 https://doi.org/10.1016/j.jclepro.2019.117689.

Shao, P., Pei, J., Tang, H., Yu, S., Yang, L., Shi, H., Yu, K., Zhang, K., Luo, X., 2021. Defect-rich porous carbon with anti-interference capability for adsorption of bisphenol A via long-range hydrophobic interaction synergized with short-range dispersion force. J. Hazard Mater. 403, 123705 https://doi.org/10.1016/j.jhazmat.2020.123705.

Shen, Y., 2015. Carbothermal synthesis of metal-functionalized nanostructures for energy and environmental applications. J. Mater. Chem. 3, 13114–13188. https://doi.org/10.1039/C5TA01228G.

Stock, P., Utzig, T., Valtiner, M., 2015. Direct and quantitative AFM measurements of the concentration and temperature dependence of the hydrophobic force law at nanoscopic contacts. J. Colloid Interface Sci. 446, 244–251. https://doi.org/10.1016/j.jcis.2015.01.032.

Sui, Q., Huang, J., Liu, Y., Chang, X., Ji, G., Deng, S., Xie, T., Yu, G., 2011. Rapid removal of bisphenol A on highly ordered mesoporous carbon. J. Environ. Sci. 23, 177–182. https://doi.org/10.1016/S1001-0742(10)60391-9.

Sun, Z., Zhao, L., Liu, C., Zhen, Y., Ma, J., 2020. Fast adsorption of BPA with high capacity based on π-π electron donor-acceptor and hydrophobicity mechanism using an in-situ sp^2 C dominant N-doped carbon. Chem. Eng. J. 381, 122510 https://doi.org/10.1016/j.cej.2019.122510.

Suzuki, T., Ohme, H., Watanabe, Y., 1994. Mechanisms of alkaline-earth metals catalyzed CO_2 gasification of carbon. Energy Fuels 8, 649–658. https://doi.org/10.1021/ef00045a021.

Tang, L., Xie, Z., Zeng, G., Dong, H., Fan, C., Zhou, Y., Wang, J., Deng, Y., Wang, J., Wei, X., 2016. Removal of bisphenol A by iron nanoparticle-doped magnetic ordered mesoporous carbon. RSC Adv. 6, 25724–25732. https://doi.org/10.1039/c5ra27710h.

Toledo, I.B., Garcia, M.A.F., Utrilla, J.R., Castilla, C.M., Fernandez, F.J.V., 2005. Bisphenol A removal from water by activated carbon. Effects of carbon characteristics and solution chemistry. Environ. Sci. Technol. 39, 6246–6250. https://doi.org/10.1021/es0481169.

Vimonses, V., Lei, S., Jin, B., Chow, C.W.K., Chris Saint, 2009. Kinetic study and equilibrium isotherm analysis of Congo Red adsorption by clay materials. Chem. Eng. J. 148, 354–364. https://doi.org/10.1016/j.cej.2008.09.009.

Wan, D., Chen, Y., Shi, Y., Liu, Y., Xiao, S., 2021. Effective adsorption of bisphenol A from aqueous solution over a novel mesoporous carbonized material based on spent bleaching earth. Environ. Sci. Pollut. Res. 28, 40035–40048. https://doi.org/10.1007/s11356-021-13596-0.

Wang, J., Deng, Z., Feng, T., Fan, J., Zhang, W.-x., 2021. Nanoscale zero-valent iron (nZVI) encapsulated within tubular nitride carbon for highly selective and stable electrocatalytic denitrification. Chem. Eng. J. 417, 129160 https://doi.org/10.1016/j.cej.2021.129160.

Wang, Q., Snyder, S., Kim, J., Choi, H., 2009. Aqueous ethanol modified nanoscale zerovalent iron in bromate reduction: synthesis, characterization, and reactivity. Environ. Sci. Technol. 43, 3292–3299. https://doi.org/10.1021/es803540b.

Wu, Y., Chen, X., Han, Y., Yue, D., Cao, X., Zhao, Y., Qian, X., 2019. Highly efficient utilization of nano-Fe(0) embedded in mesoporous carbon for activation of peroxydisulfate. Environ. Sci. Technol. 53, 9081–9090. https://doi.org/10.1021/acs.est.9b02170.

Xie, L., Yang, D., Lu, Q., Zhang, H., Zeng, H., 2020. Role of molecular architecture in the modulation of hydrophobic interactions. Curr. Opin. Colloid Interface Sci. 47, 58–69. https://doi.org/10.1016/j.cocis.2019.12.001.

Xu, Z., Ding, L., Long, Y., Xu, L., Wang, L., Xu, C., 2011. Preparation and evaluation of superparamagnetic surface molecularly imprinted polymer nanoparticles for selective extraction of bisphenol A in packed food. Anal. Methods 3, 1737. https://doi.org/10.1039/C1AY05206C.

Zhang, S., Shao, T., Bekaroglu, S.S.K., Karanfil, T., 2010. Adsorption of synthetic organic chemicals by carbon nanotubes: effects of background solution chemistry. Water Res. 44, 2067–2074. https://doi.org/10.1016/j.watres.2009.12.017.

Zhou, A., Wu, X., Chen, W., Liao, L., Xie, P., 2020. Fabrication of hydrophobic/hydrophilic bifunctional adsorbent for the removal of sulfamethoxazole and bisphenol A in Water. J. Environ. Chem. Eng. 8 https://doi.org/10.1016/j.jece.2020.104161.

Zhou, Y., Gao, B., Zimmerman, A.R., Chen, H., Zhang, M., Cao, X., 2014. Biochar-supported zerovalent iron for removal of various contaminants from aqueous solutions. Bioresour. Technol. 152, 538–542. https://doi.org/10.1016/j.biortech.2013.11.021.